1. General

The UV-vis spectra were recorded using a JASCO V-670 spectrometer equipped with a thermal controller. Atomic force microscopy (AFM) images were acquired in air using a Shimadzu SPM 9600 microscope (dynamic mode). Each sample was cast onto mica and dried for 6 h under reduced pressure prior to observation. Dynamic light scattering (DLS) data were obtained using a Malvern Zetasizer Nano ZS. All reagents and solvents were purchased from Tokyo Chemical Industry, Wako Pure Chemical Industries, and Nacalai Tesque.

2. Microflow design

A glass microflow chip was used in this study. The microchannel was designed with a depth of 45 μm, top width of 190 μm, bottom width of 100 μm, and total channel length of 60 mm.

3. Experimental section

Syntheses of H_2TPPS_2-NHCO-EG_x (x = 2, 4, 6, 8, 18) porphyrin derivatives

The H_2TPPS_2-NHCO-EG_x (x = 2, 4, 6, 8, and 18) porphyrin derivatives were synthesized according to previously reported procedures.[1,2]

General experiments using microflow device

A solution was introduced into the microflow channel through a Teflon capillary (inner mm diameter: 300 μm; length: 80 mm). The flow rate was adjusted using a syringe pump. The eluted solution was collected in a vial through a Teflon capillary (inner diameter: 300 μm; length: 80 mm) and subjected to spectroscopic and microscopic observations.

Preparation of H_2TPPS_4 supramolecular polymer

A solution H_2TPPS_2 in ultrapure water (800 μM) was mixed with aqueous HCl (pH 2) in a vial. The final concentration was adjusted to 40 μM. The solution was allowed to stand for 70 min. As revealed in Fig. S1, the solution contained short nanofibers with an average length of 0.85 μm. This solution was used as a stock solution for fabricating the H_2TPPS_4 supramolecular polymer.

Preparation of H_2TPPS_2-NHCO-EG_x monomer solution[1,2]

A MeOH solution of the H_2TPPS_2-NHCO-EG_x (x = 2, 4, 6, 8, and 18) porphyrin derivative was mixed with an aqueous HCl solution by adjusting the final water/MeOH solvent

composition to 9/1. The final concentration was adjusted to 30, 50, and 70 μM. These solutions were used as stock solutions for the H_2TPPS_2-NHCO-EG_x monomer.

Supramolecular copolymerization in a vial

A H_2TPPS_2-NHCO-EG_x monomer (30, 50, or 70 μM) solution in a water/MeOH mixture was added to an acidic aqueous solution of the pre-prepared H_2TPPS_4 supramolecular polymer (40 μM). The final water/MeOH ratio was adjusted to 96/4 (v/v). The solution of the H_2TPPS_4 supramolecular polymer was diluted by 3/5 (i.e., the final concentration was 24 μM). The final monomer concentration was 12, 20, or 28 μM.

Supramolecular copolymerization in microflow channel

The acidic aqueous solution of the H_4TPPS_4 supramolecular polymer (40 μM) was injected into the central inlet of the cross-type microchannel, with a flow rate of 60 μL/min. A solution of H_2TPPS_2-NHCO-EG_x monomer was injected from two lateral inlets, with a flow rate of 20 μL/min, giving a total flow rate of 100 μL/min. The concentration of the monomer solution was varied from 30, 50, to 70 μM while fixing the polymer concentration. After elusion from the microflow channel, the H_4TPPS_4 supramolecular polymer solution was diluted by 3/5 (i.e., 24 μM). Likewise, the monomer solution was diluted by 2/5 (i.e., 12, 20, 28 μM). The eluted solutions were collected in a vial and subjected to UV-vis and DLS measurements, and AFM observations.

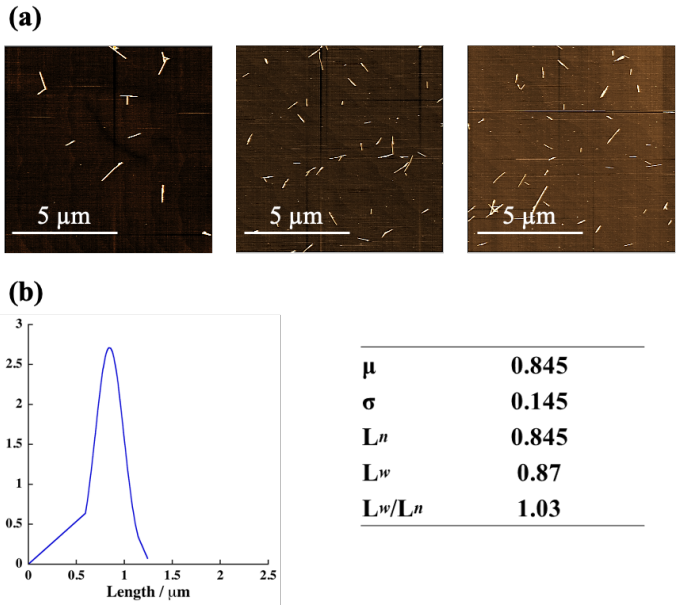

μ	**0.845**
σ	**0.145**
L_n	**0.845**
L_w	**0.87**
L_w/L_n	**1.03**

Fig. S1. AFM images of the pre-prepared H_4TPPS_4 supramolecular polymers and characteristics of the resultant polymers, measured from the AFM images of at least 300 fibers; μ: mean length (μm); s: standard deviation of measured lengths; *L*n: number-average length; *L*w: weight-average length; *L*w/*L*n: dispersity.

4. Concentration-dependent supramolecular copolymerization in microflow channel

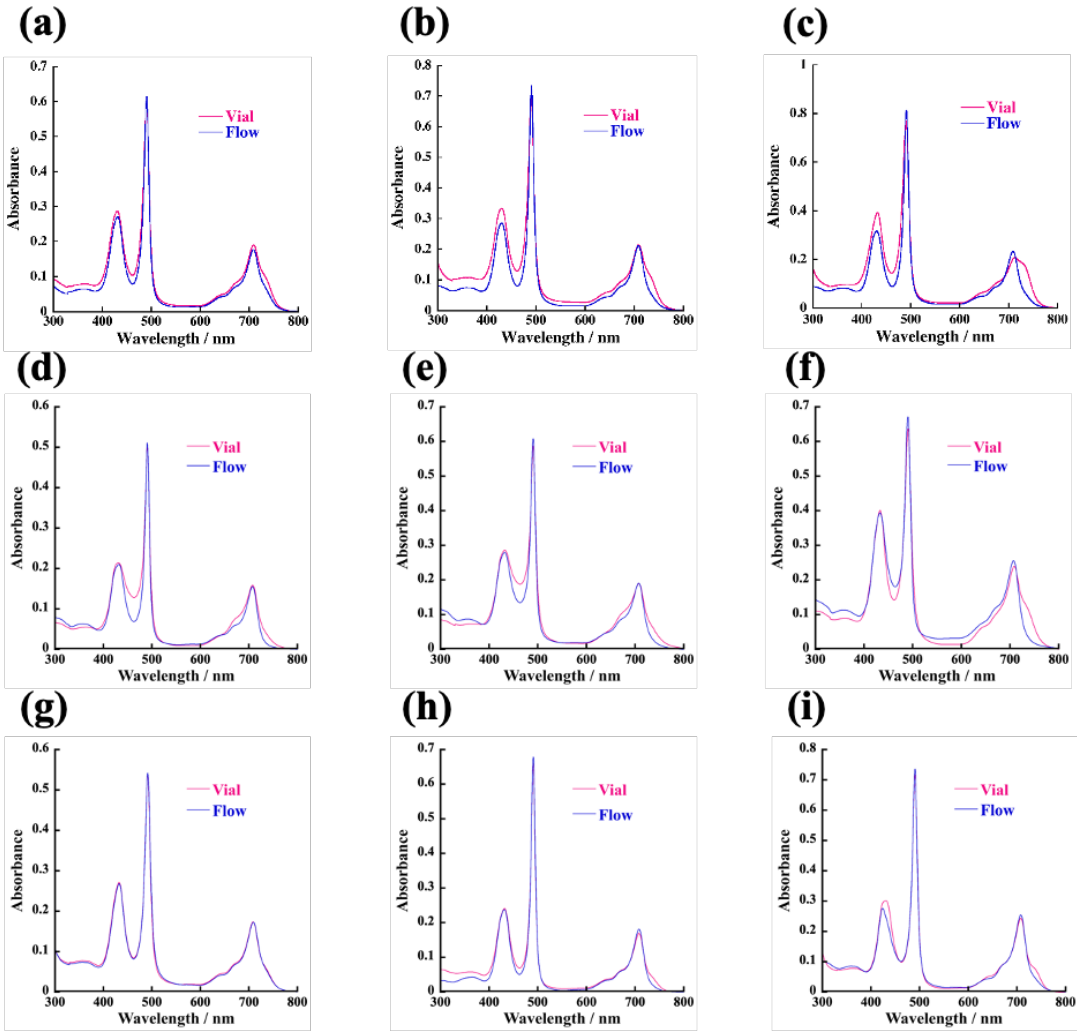

Fig. S2. Comparison of UV-vis spectra of vial (magenta lines) and flow (blue lines) samples upon supramolecular polymerization; (a–c) addition of (a) 30, (b) 50, and (c) 70 μM of H_2TPPS_2-NHCO-EG_2; (d–f) addition of (d) 30, (e) 50, and (f) 70 μM of H_2TPPS_2-NHCO-EG_4; (g–i) addition of (g) 30, (h) 50, and (i) 70 μM of H_2TPPS_2-NHCO-EG_6.

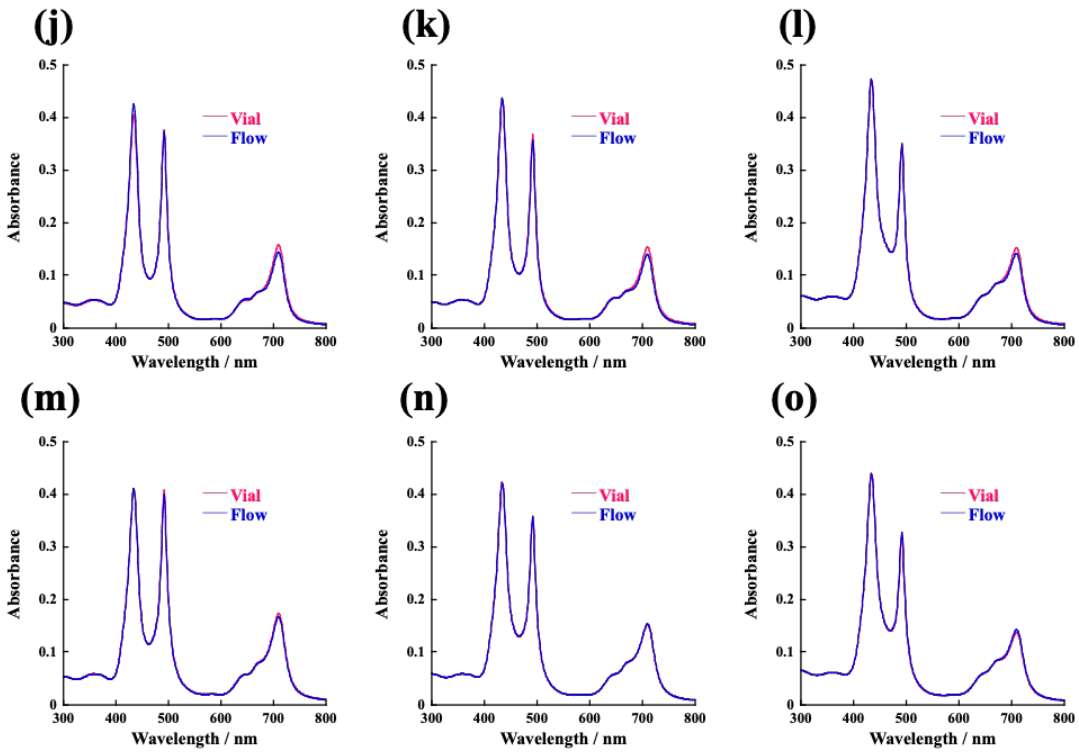

Fig. S2 continued. (j–l) addition of (a) 30, (b) 50, and (c) 70 μM of H_2TPPS_2-NHCO-EG_8; (m–o) addition of (d) 30, (e) 50, and (f) 70 μM of H_2TPPS_2-NHCO-EG_{18} [1.0 mm cell, r.t., water/MeOH; 96/4 (v/v), the concentration of injected H_2TPPS_4 monomer was fixed at 40 μM].

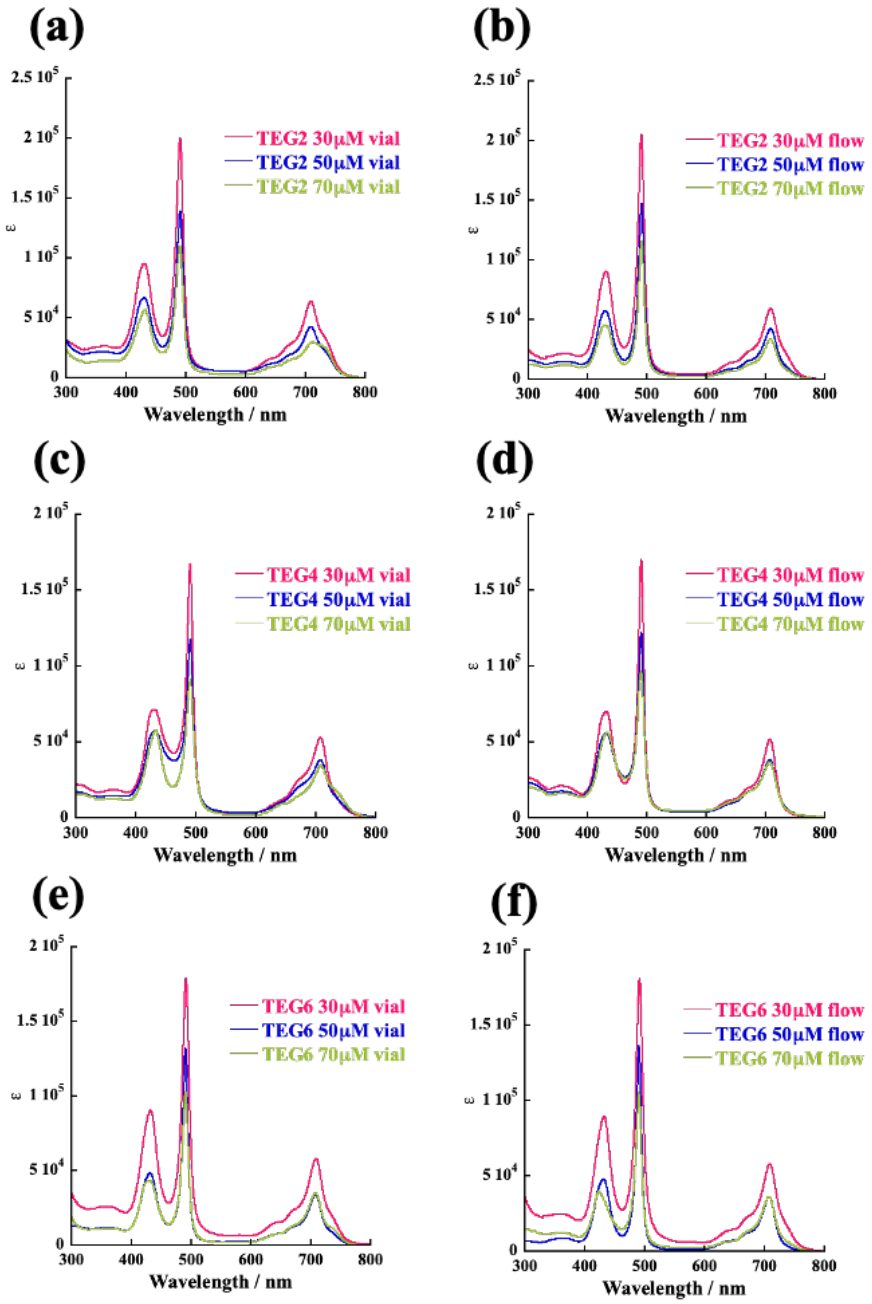

Fig. S3. Comparison of concentration-dependent UV-vis spectral changes upon supramolecular polymerization in vial (a, c, e, g, i) and flow channel (b, d, f, h, j); upon addition of (a, b) H_2TPPS_2-NHCO-EG_2, (c, d) H_2TPPS_2-NHCO-EG_4, and (e, f) H_2TPPS_2-NHCO-EG_6.

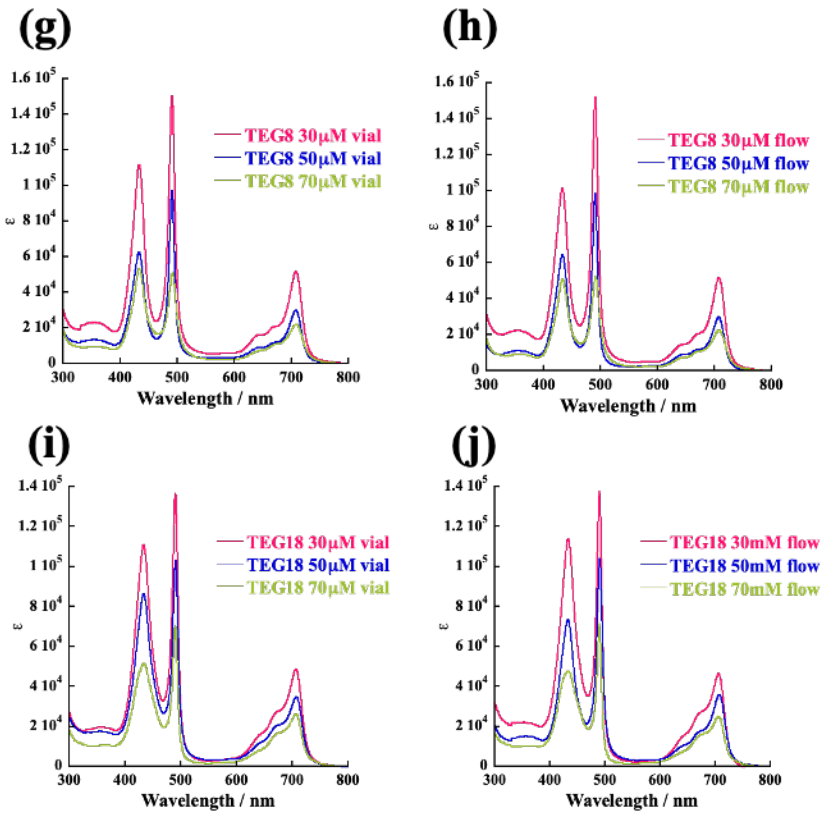

Fig. S3 continued. (g, h) H_2TPPS_2-NHCO-EG_8, (i, j) H_2TPPS_2-NHCO-EG_{18} [1.0 mm cell, r.t., water/MeOH; 96/4 (v/v), the inset values represent the concentration of added monomer].

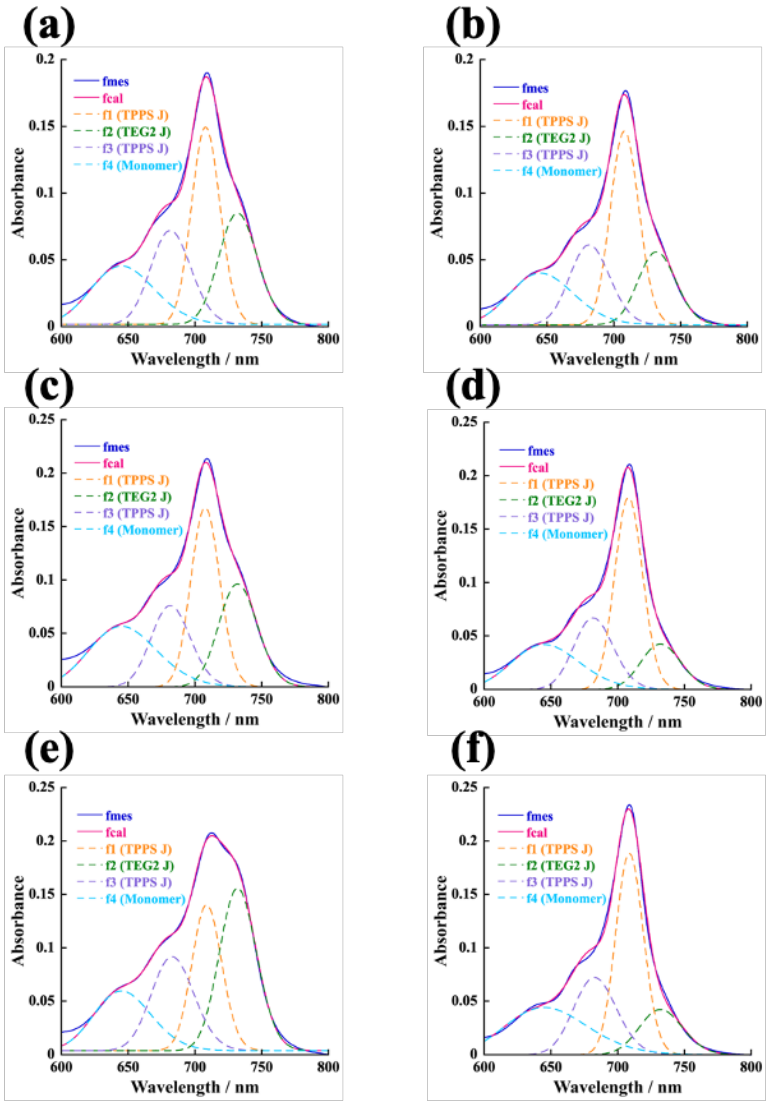

Fig. S4. Deconvoluted UV-vis spectra upon supramolecular polymerization in vial (a, c, e) and flow channel (b, d, f) upon addition of (a, b) 30, (c, d) 50, and (e, f) 70 μM of H_2TPPS_2-NHCO-EG_2 [1.0 mm cell, r.t., the concentration of injected solution of H_4TPPS_4 supramolecular polymer was fixed at 40 μM; for the inset; blue lines: measured spectra, magenta: calculated spectra, f1 orange: H_4TPPS_4 J-aggregate, f2 green: H_4TPPS_2-NHCO-EG_2 aggregate, f3 purple: second band of H_4TPPS_4 J-aggregate, f4 light-blue: unreacted H_4TPPS_4 monomer].

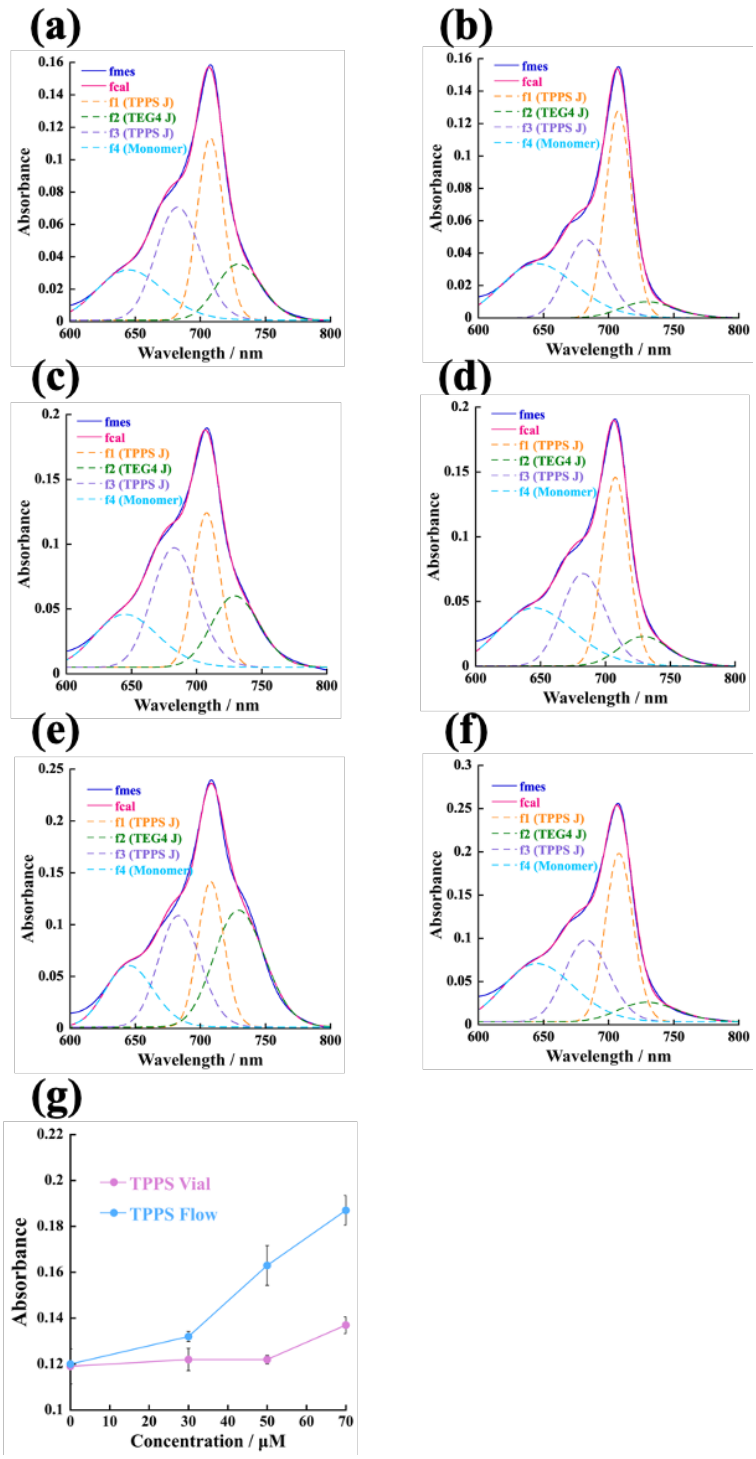

Fig. S5. Deconvoluted UV-vis spectra upon supramolecular polymerization in vial (a, c, e) and flow channel (b, d, f) upon addition of (a, b) 30, (c, d) 50, and (e, f) 70 μM of H_2TPPS_2-NHCO-EG_4 [1.0 mm cell, r.t., the concentration of injected solution of H_4TPPS_4 supramolecular polymer was fixed at 40 μM. Inset—blue lines: measured spectra, magenta: calculated spectra, f1 orange: H_4TPPS_4 J-aggregate, f2 green: H_4TPPS_4-NHCO-EG_4 aggregate, f3 purple: second band of H_4TPPS_4 J-aggregate, f4 light-blue: unreacted H_4TPPS_4 monomer]. (g) Plots of absorbance at 708 nm with respect to monomer concentration (for plots at 732 nm, see Fig. S7b).

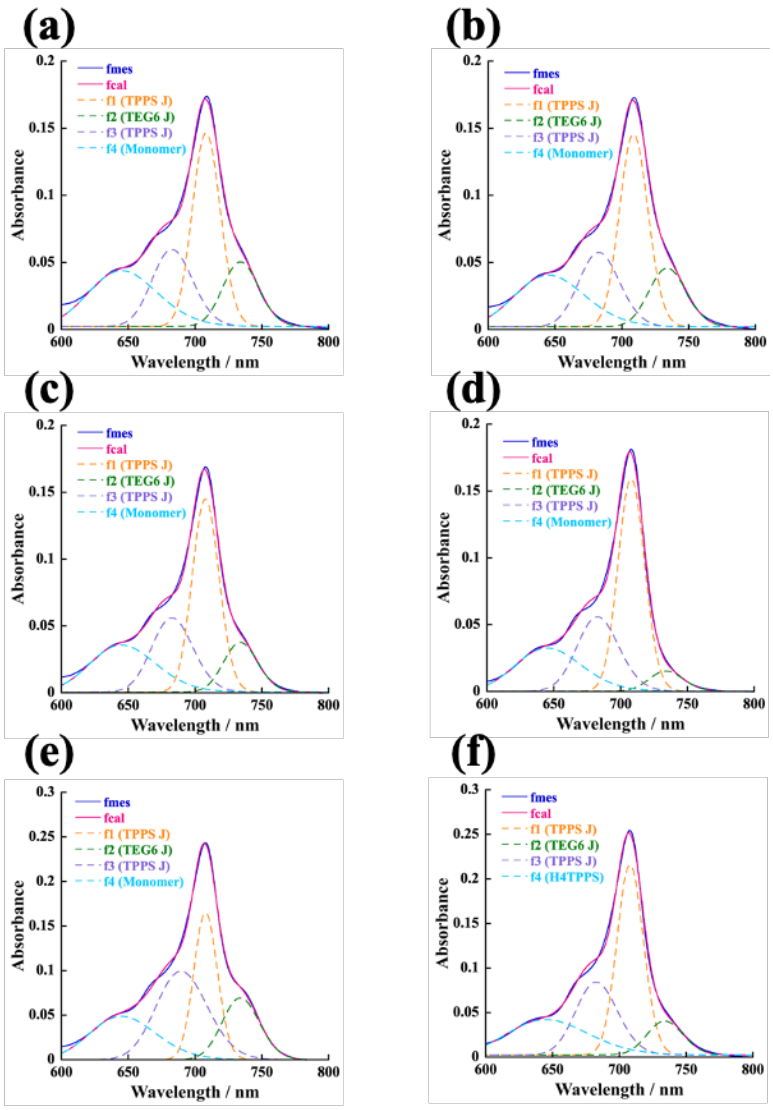

Fig. S6. Deconvoluted UV-vis spectra upon supramolecular polymerization in vial (a, c, e) and in flow channel (b, d, f) upon addition of (a, b) 30, (c, d) 50, (e, f) 70 μM of H_2TPPS_2-NHCO-EG_6 [1.0 mm cell, r.t., the concentration of injected solution of H_4TPPS_4 supramolecular polymer was fixed at 40 μM; inset—blue lines: measured spectra, magenta: calculated spectra, f1 orange: H_4TPPS_4 J-aggregate, f2 green: H_4TPPS_2-NHCO-EG_6 aggregate, f3 purple: second band of H_4TPPS_4 J-aggregate, f4 light-blue: unreacted H_4TPPS_4 monomer].

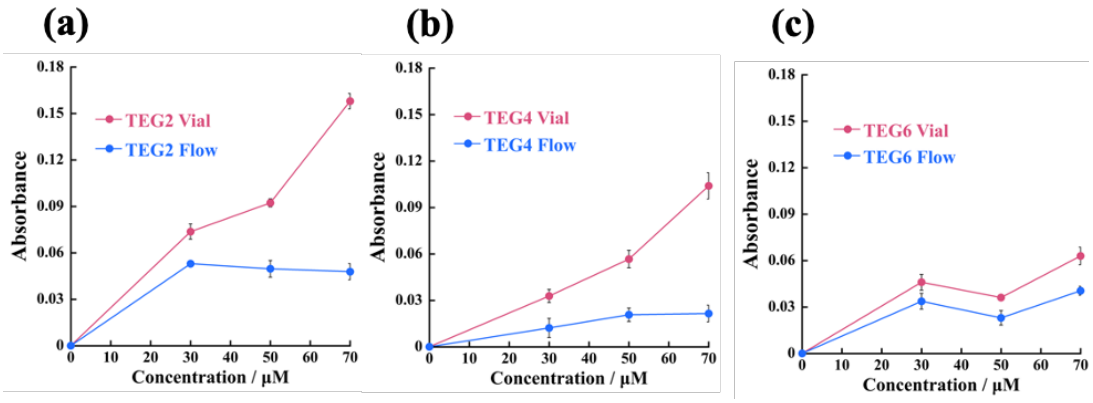

Fig. S7. Plots of absorbance at 732 nm (corresponding to homopolymer) versus monomer concentration (red line: vial sample, blue line: flow sample) upon addition of (a) H_2TPPS_2-NHCO-EG_2, (b) -EG_4, and (c) -EG_6.

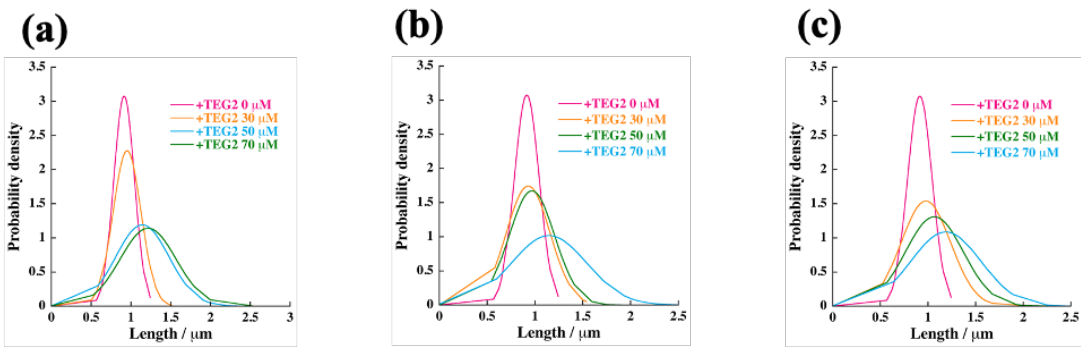

Fig. S8. (a–c) Length distributions of supramolecular polymers. The data were collected from three different samples, a, b, and c. For each sample, the length of the nanofibers was measured from the AFM images of at least 100 fibers (values in inset: concentrations of added monomer).

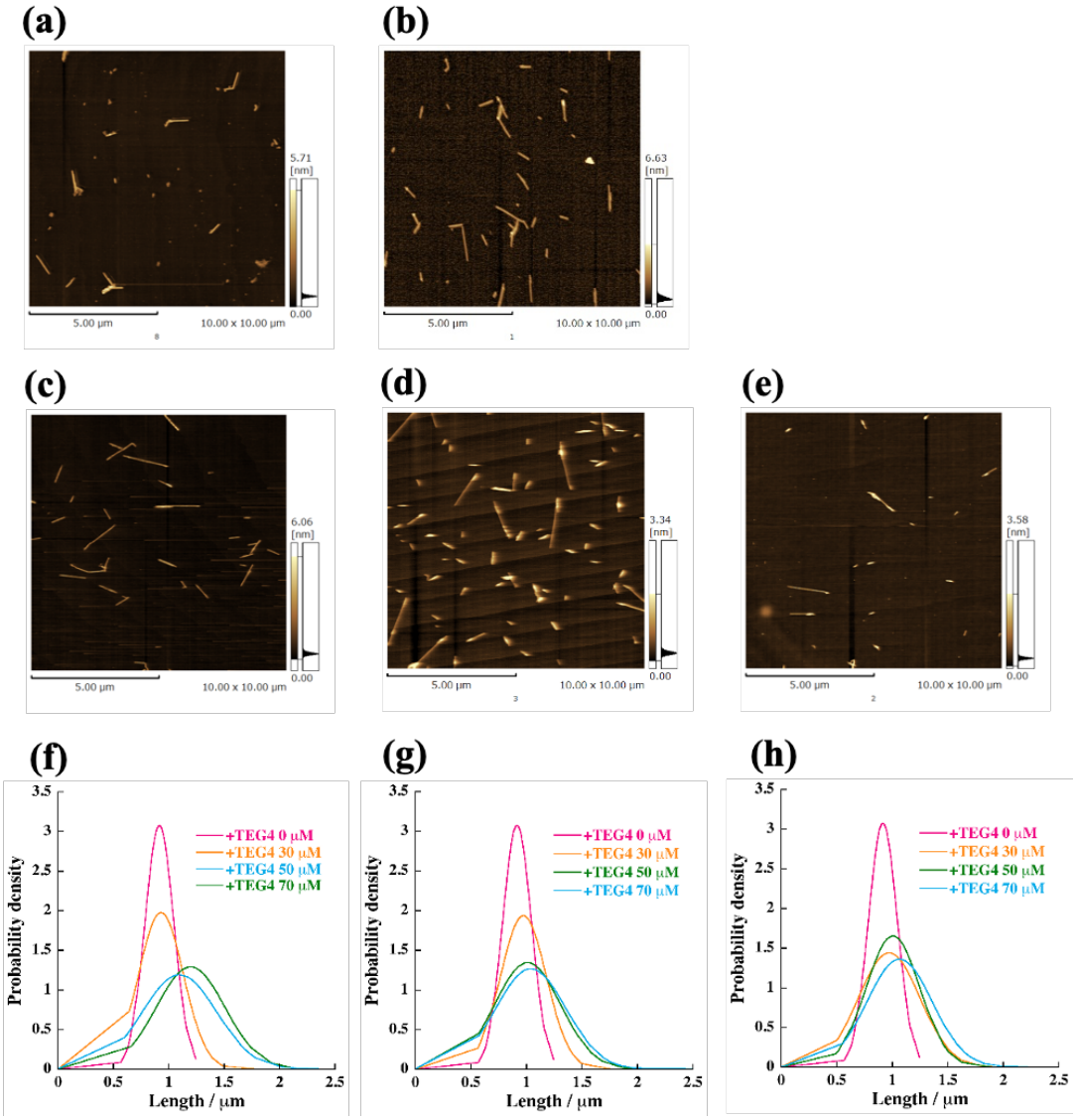

Fig. S9. (a–d) Concentration-dependent AFM images of H_4TPPS_4/-EG_4 block copolymer prepared upon addition of (a) 0, (b) 30, (c) 50, and (d) 70 µM of H_2TPPS_2-NHCO-EG_4; (e) AFM image of nanofibers prepared in vial upon addition of 70 µM of H_2TPPS_2-NHCO-EG_4; (f–h) length distributions of supramolecular polymers. The data were collected from three different samples, f, g, and h. For each sample, the length of the nanofibers was measured from the AFM images of at least 100 fibers (values in inset: concentrations of added monomer).

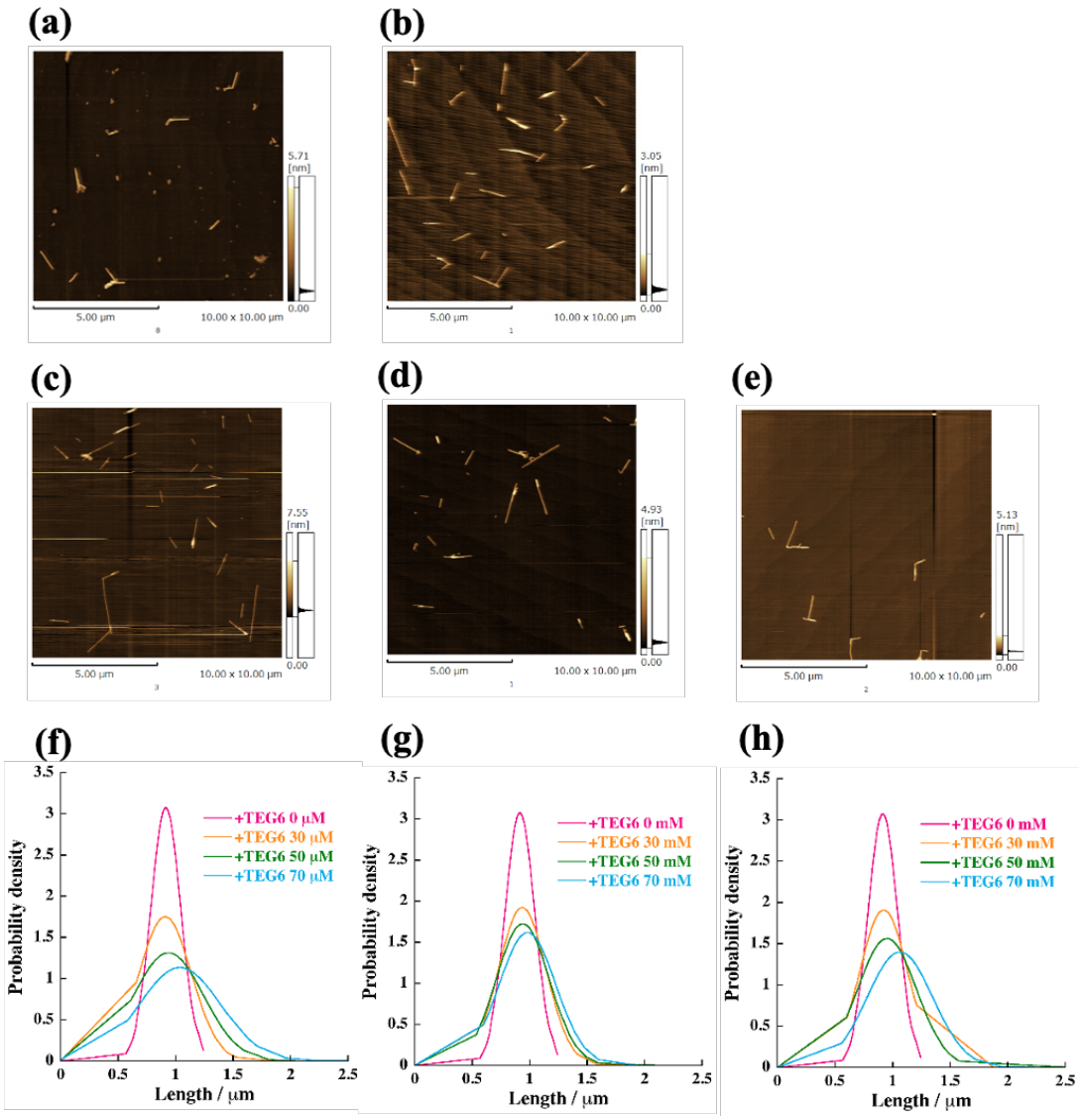

Fig. S10. (a–d) Concentration-dependent AFM images of H_4TPPS_4/-EG_6 block copolymer prepared upon addition of (a) 0, (b) 30, (c) 50, and (d) 70 µM of H_2TPPS_2-NHCO-EG_6; (e) AFM image of nanofibers prepared in vial upon addition of 70 µM of H_2TPPS_2-NHCO-EG_6; (f–h) length distributions of supramolecular polymers. The data were collected from three different samples, f, g, and h. For each sample, the length of the nanofibers was measured from the AFM images of at least 100 fibers (values in inset: concentrations of added monomer).

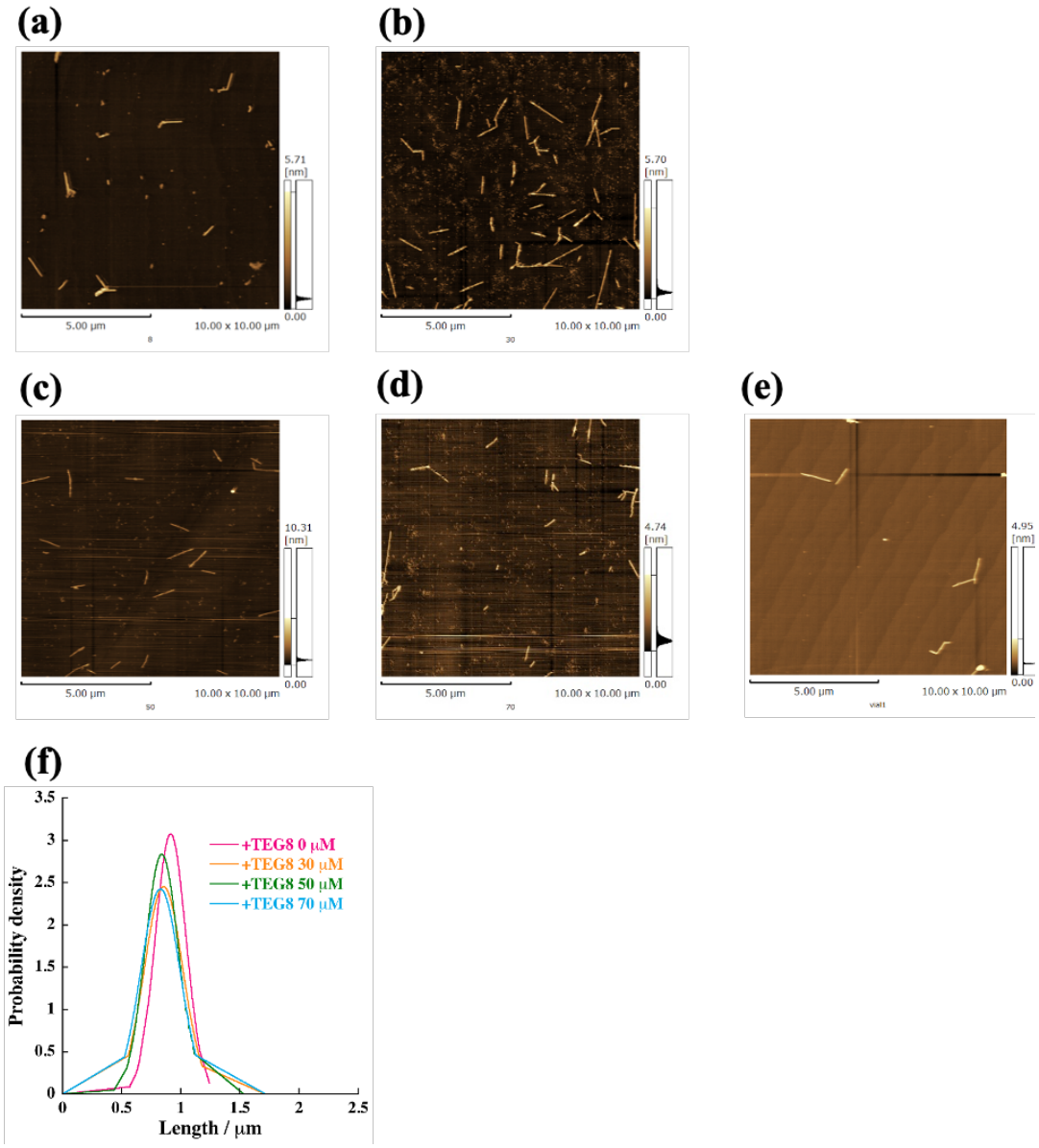

Fig. S11. (a–d) Concentration-dependent AFM images of supramolecular polymer prepared upon addition of (a) 0, (b) 30, (c) 50, and (d) 70 µM of H_2TPPS_2-NHCO-EG_8; (e) AFM image of nanofibers prepared in vial upon addition of 70 µM of H_2TPPS_2-NHCO-EG_8; (f) length distributions of supramolecular polymers measured from AFM images of at least 300 fibers (values in inset: concentrations of added monomer).

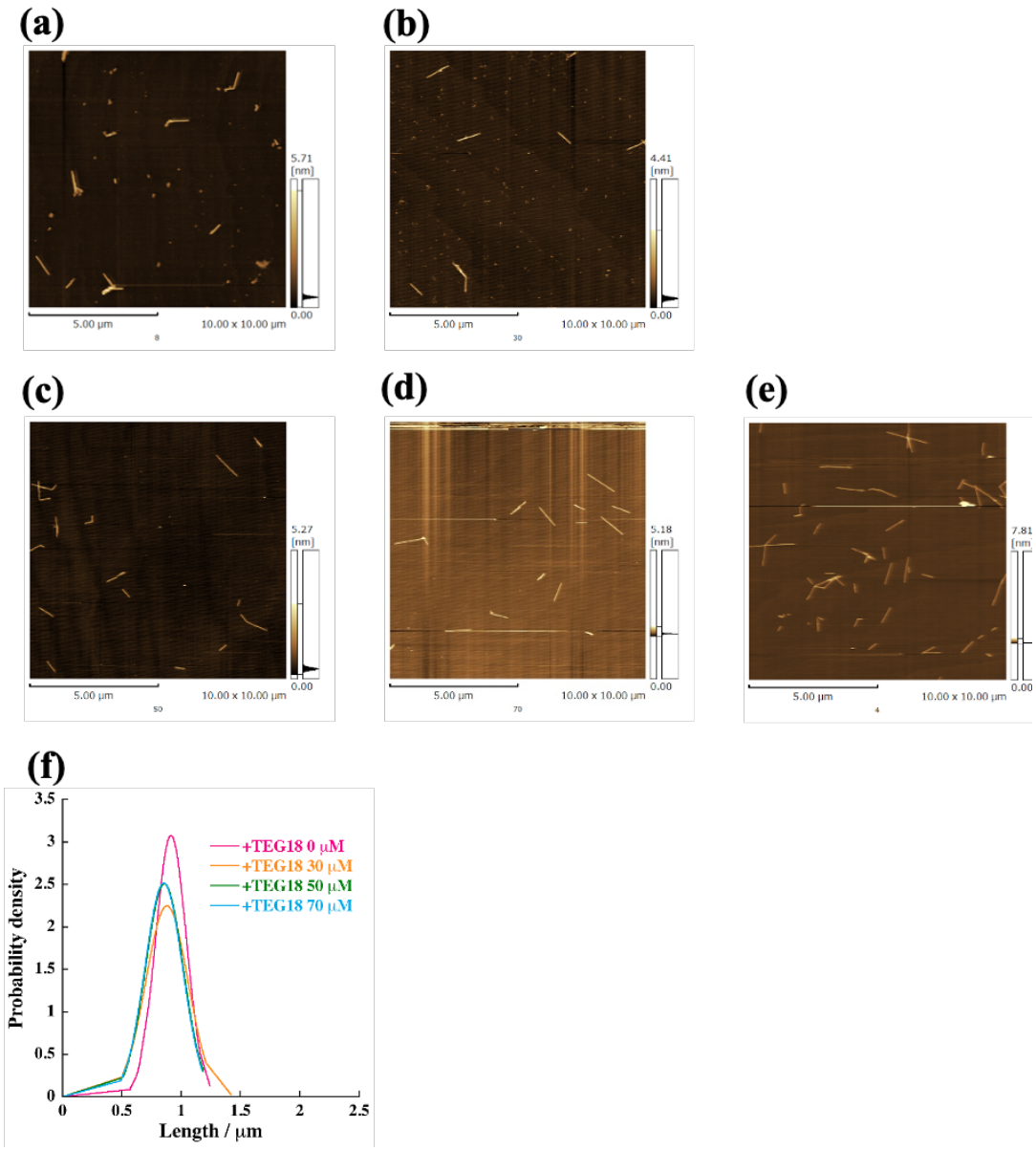

Fig. S12. (a–d) Concentration-dependent AFM images of supramolecular polymer prepared upon addition of (a) 0, (b) 30, (c) 50, and (d) 70 µM of H_2TPPS_2-NHCO-EG_{18}; (e) AFM image of nanofibers prepared in vial upon addition of 70 µM of H_2TPPS_2-NHCO-EG_{18}; (f) length distributions of supramolecular polymers measured from AFM images of at least 300 fibers (values in inset: concentrations of added monomer).

.

5. Self-assembly behaviors of H_2TPPS_2-NH-EG_x monomers in microflow channel

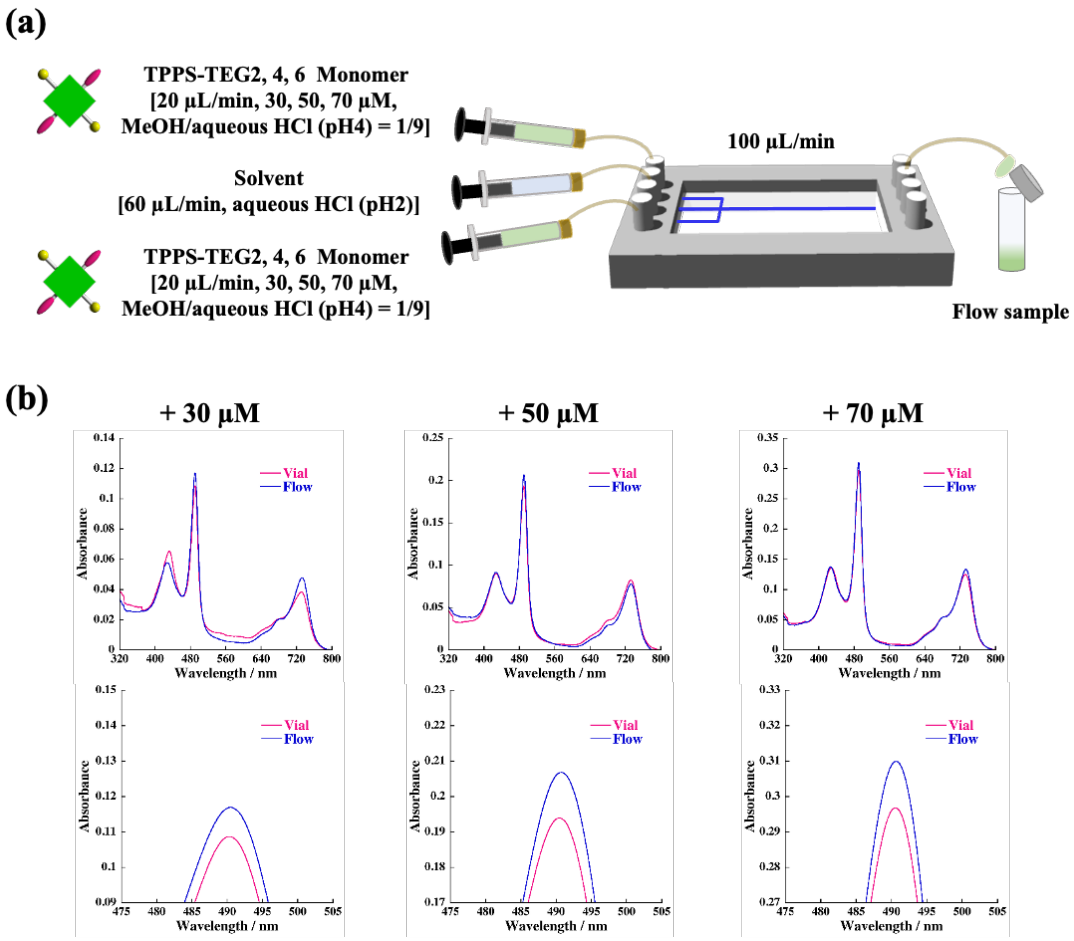

Fig. S13. (a) Schematic set-up for the present experiment; (b) concentration dependence of UV–vis spectra of the eluted solution (blue lines) upon addition of H_2TPPS_2-NHCO-EG_2.

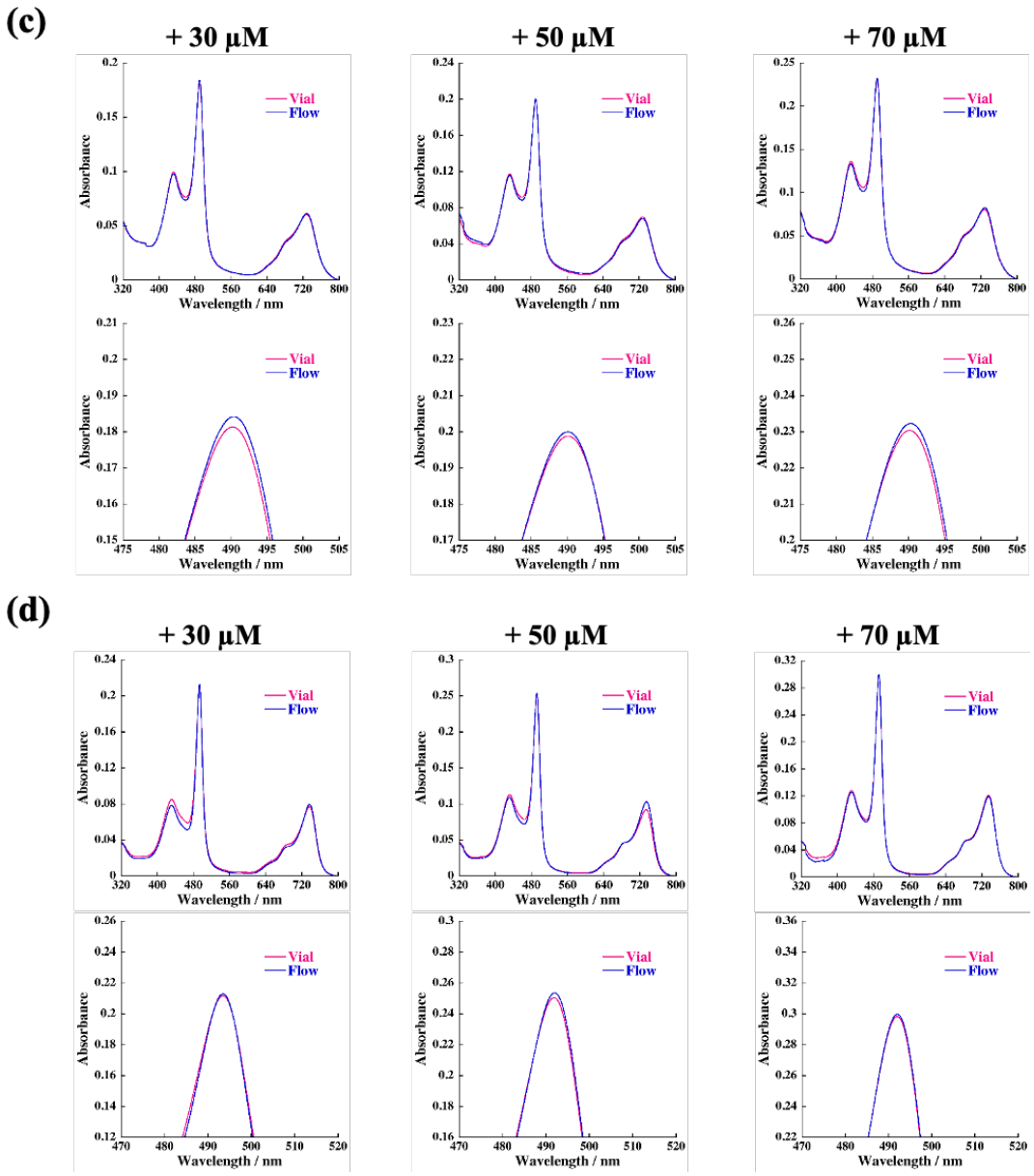

Fig. S13 continued. (c, d) concentration dependence of UV–vis spectra of the eluted solution (red lines) upon addition of (c) H_2TPPS_2-NHCO-EG_4 and (d) -EG_6 (red lines represent the corresponding vial sample) [1.0 mm cell, r.t.].

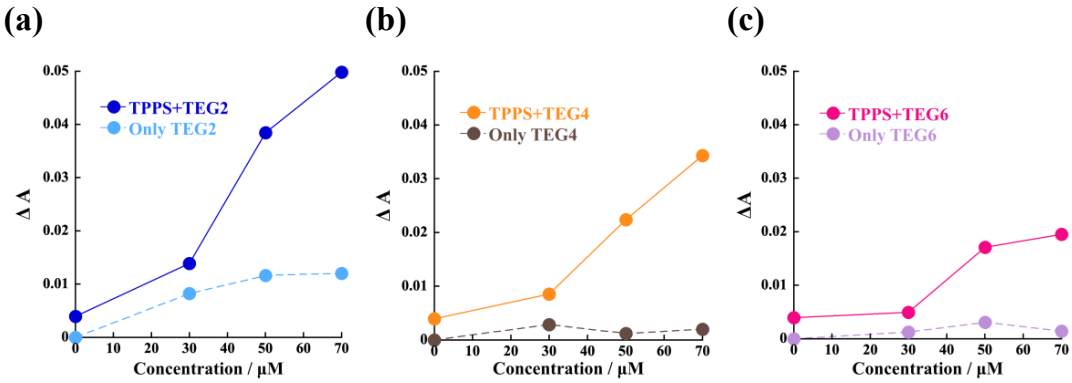

Fig. S14. Comparison of plots of Δ*A* at 490 nm against H_2TPPS_2-NHCO-EG_x monomer concentration; solid lines correspond to the degree of supramolecular copolymerization and dotted lines represent supramolecular polymerization of monomer in microflow channel, obtained from the data in Fig. S13; (a) H_2TPPS_2-NHCO-EG_2, (b) -EG_4, and (c) -EG_6.

6. Flow-rate-dependent-self-assembly of series of H_2TPPS_2-NHCO-EG_x monomers in microflow channel

We investigated the inherent reactivity of each monomer (H_2TPPS_2-NHCO-EGx) under laminar flow. According to the setup for supramolecular copolymerization, a solution of the monomer was injected from the two-sided inlet into the microflow channel, and aqueous HCl was injected from the central leg instead of a solution of the H_4TPPS_4 supramolecular polymer. The UV-vis spectra of the eluted solutions revealed a clear steric effect of the EG units on the self-assembly ability; that is, the characteristic band corresponding to J-aggregates appeared only for the H_2TPPS_2-NHCO-EG_2 and -EG_4 monomers. In the case of H_2TPPS_2-NHCO-EG_6 having medium-sized peripherals, a small amount of J-aggregate was formed in addition to a significant amount of the protonated form that remained unreacted.

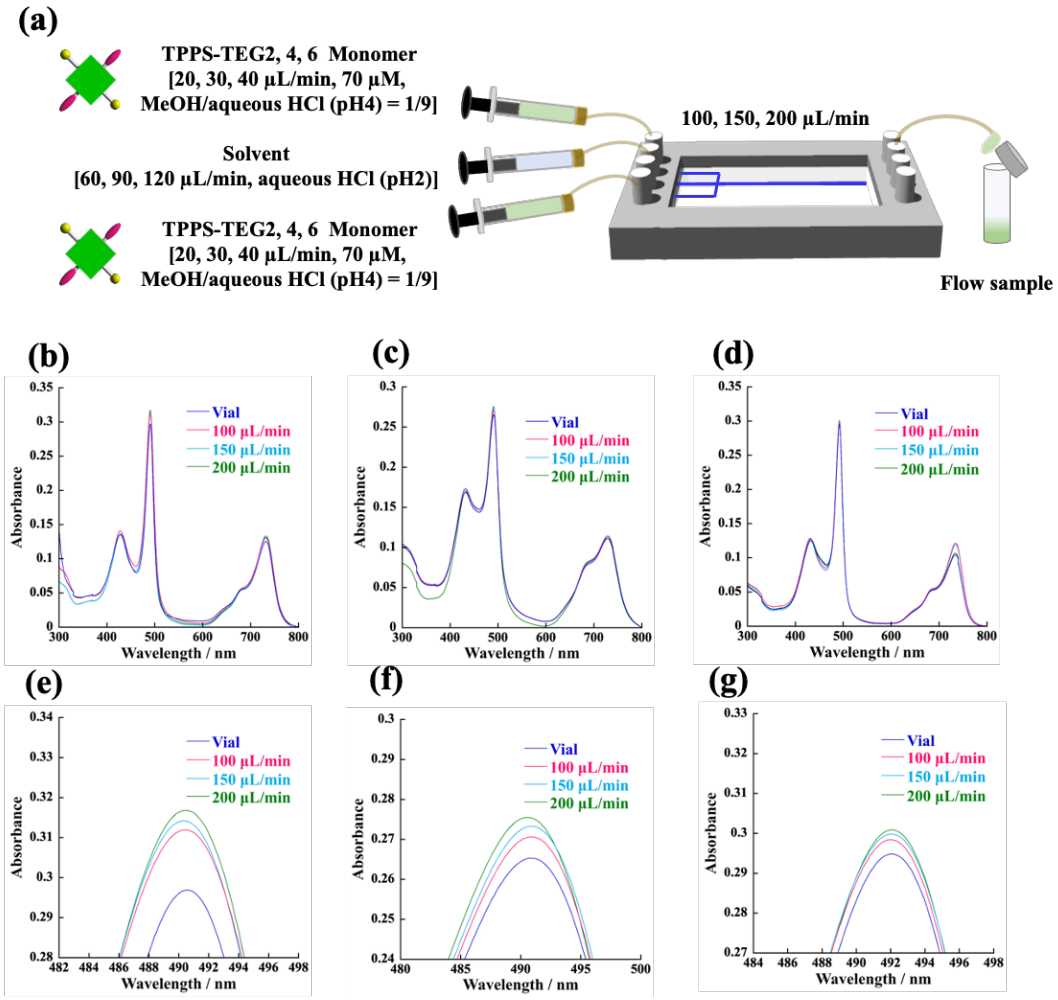

Fig. S15. (a) Schematic set-up for the present experiment; (b-d) flow rate dependence of UV–vis spectra of the eluted solution; (e), (f) and (g) are enlarged spectra of (b), (c), and (d), respectively [the inset values represent the flow rates (blue lines correspond to the vial sample), 1.0 mm cell; r.t.].

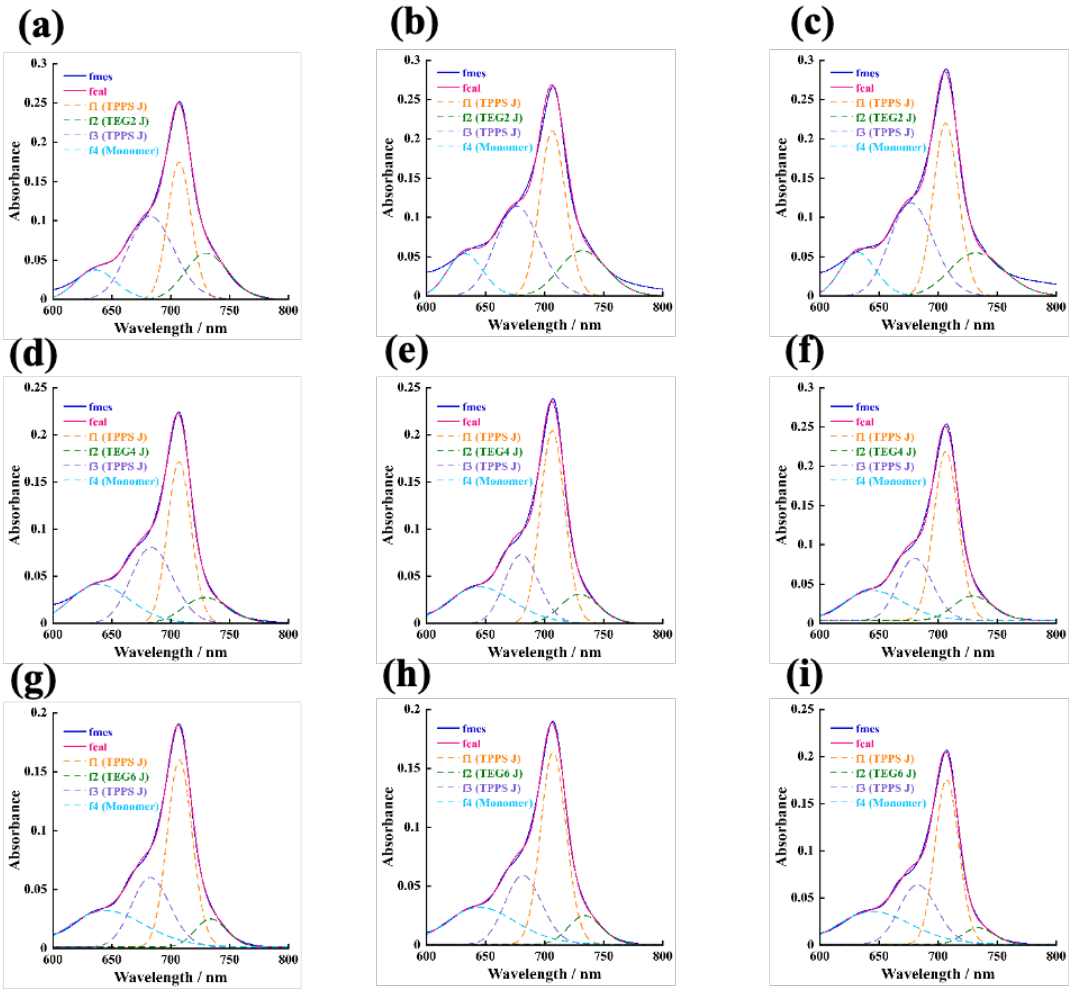

Fig. S16. Deconvoluted UV-vis spectra of the eluted solution collected at rate of (a, d, g) 100, (b, e, h) 150, and (c, f, i) 200 μL/min in the presence of 70 μM (a, b, c) H_2TPPS_2-NHCO-EG_2, (d, e, f) H_2TPPS_2-NHCO-EG_4, and (g, h, i) H_2TPPS_2-NHCO-EG_6 monomer [1.0 mm cell, r.t., concentration of injected solution of H_4TPPS_4 supramolecular polymer was fixed at 40 μM. Inset—blue lines: measured spectra, magenta: calculated spectra, f1 orange: H_4TPPS_4 J-aggregate, f2 green: H_4TPPS_2-NHCO-EG_x (x = 2, 4, or 6) aggregate, f3 purple: second band of H_4TPPS_4 J-aggregate, f4 light-blue: unreacted H_4TPPS_4 monomer].

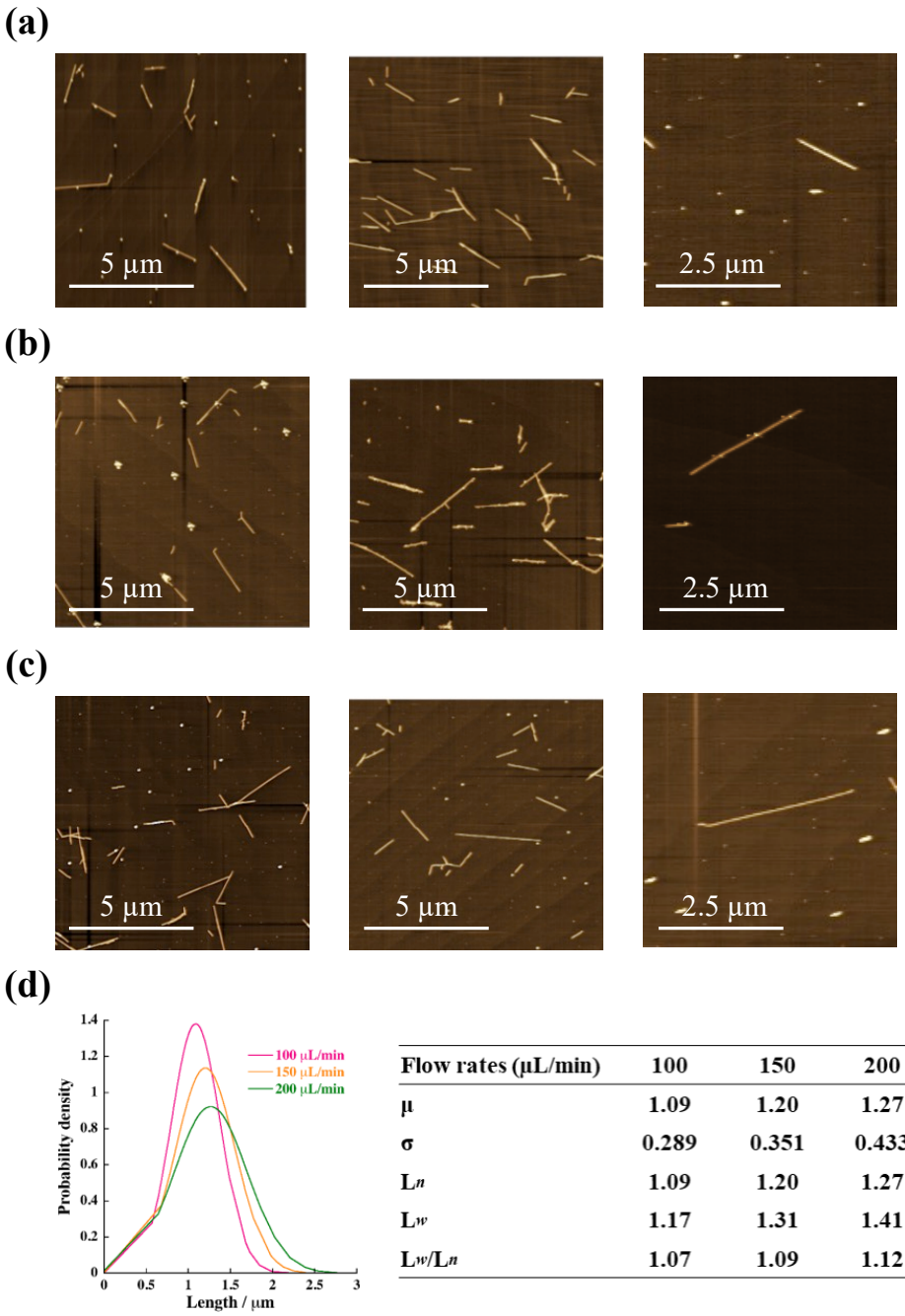

Flow rates (μL/min)	100	150	200
μ	1.09	1.20	1.27
σ	0.289	0.351	0.433
L_n	1.09	1.20	1.27
L_w	1.17	1.31	1.41
L_w/L_n	1.07	1.09	1.12

Fig. S17. Flow-rate dependence of AFM images of supramolecular diblock copolymers obtained upon injection of H_2TPPS_2-NHCO-EG_2 solution at (a) 100, (b) 150, and (c) 200 μL/min; (d) length distributions of supramolecular diblock copolymers measured from AFM images of at least 300 fibers (values in inset represent flow rates) and characteristics of the resultant polymers; μ: mean length (μm); s: standard deviation of measured lengths; *L*n: number-average length; *L*w: weight-average length; *L*w/*L*n: dispersity.

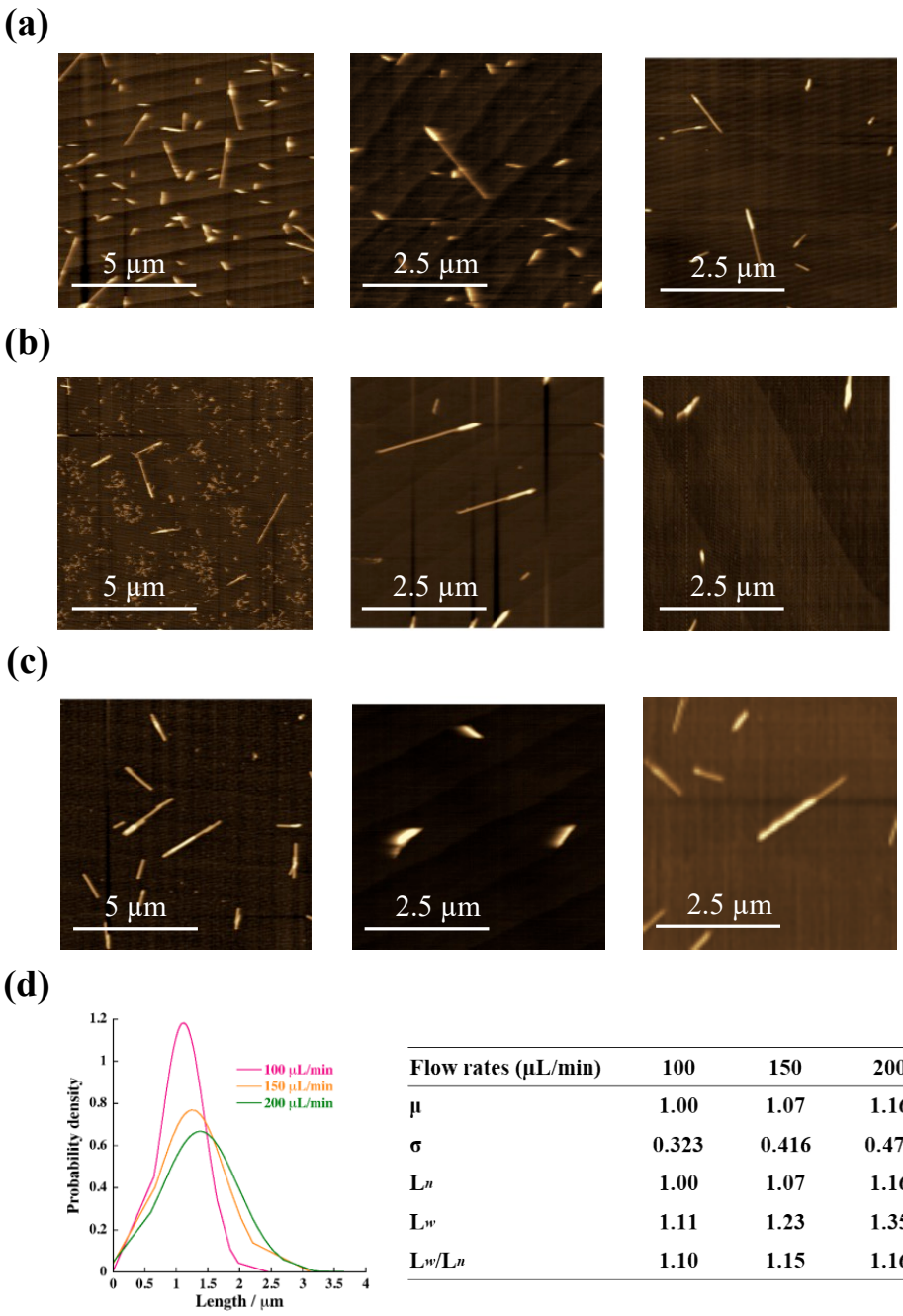

Flow rates (μL/min)	100	150	200
μ	1.00	1.07	1.16
σ	0.323	0.416	0.470
L_n	1.00	1.07	1.16
L_w	1.11	1.23	1.35
L_w/L_n	1.10	1.15	1.16

Fig. S18. Flow-rate dependence of AFM images of supramolecular diblock copolymers obtained upon injection of H_2TPPS_2-NHCO-EG_4 solution at (a) 100, (b) 150, and (c) 200 μL/min; (d) length distributions of supramolecular diblock copolymers measured from AFM images of at least 300 fibers (values in inset represent flow rates) and characteristics of the resultant polymers; μ: mean length (μm); s: standard deviation of measured lengths; *L*n: number-average length; *L*w: weight-average length; *L*w/*L*n: dispersity.

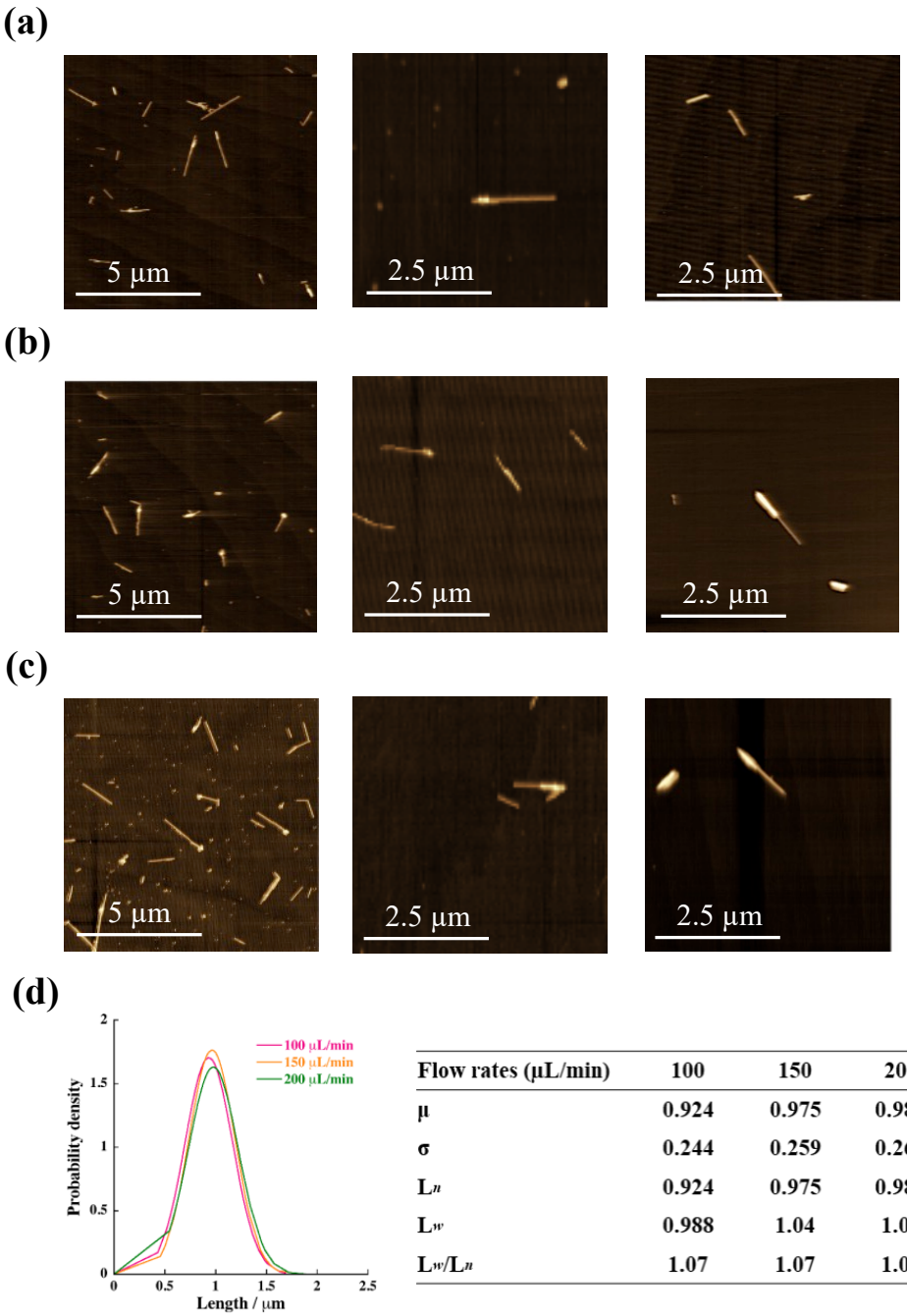

Flow rates (μL/min)	100	150	200
μ	0.924	0.975	0.989
σ	0.244	0.259	0.265
L_n	0.924	0.975	0.989
L_w	0.988	1.04	1.06
L_w/L_n	1.07	1.07	1.07

Fig. S19. Flow-rate dependence of AFM images of supramolecular diblock copolymers obtained upon injection H_2TPPS_2-NHCO-EG_6 solution at (a) 100, (b) 150, and (c) 200 μL/min; (d) length distributions of supramolecular diblock copolymers measured from AFM images of at least 300 fibers (values in inset represent flow rates) and characteristics of the resultant polymers; μ: mean length (μm); s: standard deviation of measured lengths; *L*n: number-average length; *L*w: weight-average length; *L*w/*L*n: dispersity.

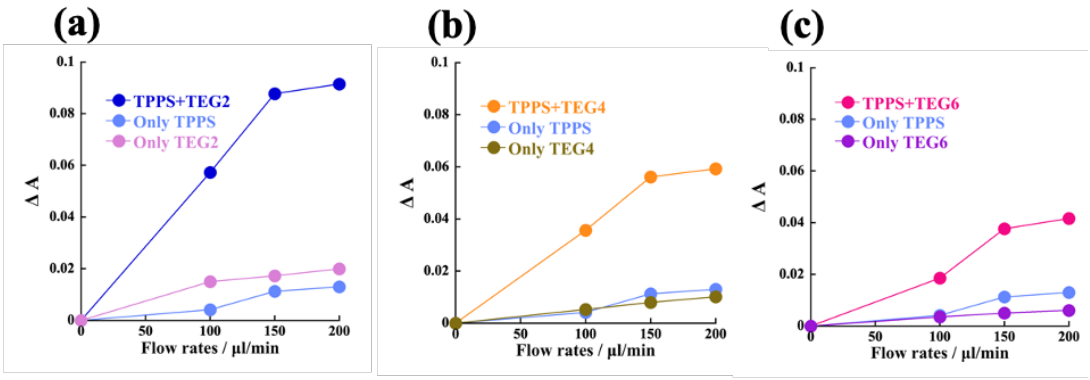

Fig. S20. Comparative plots of ΔA at 490 nm with respect to flow rate; flow-rate-dependent supramolecular copolymerization of H_4TPPS_4 supramolecular polymer with (a) H_2TPPS_2-NHCO-EG_2 (blue line), (b) H_2TPPS_2-NHCO-EG_4 (orange line), and (c) H_2TPPS_2-NHCO-EG_6 (magenta line) monomers; in each spectrum, ΔA values obtained upon solely injecting H_4TPPS_4 supramolecular polymer or H_2TPPS_2-NHCO-EG_x (x = 2, 4, or 6) monomer are also plotted for comparison.

To gain further insights into the detailed extension mechanism, the rates of the reaction of the parent H_4TPPS_4 polymers with the H_2TPPS_2-NHCO-EG_4 or -EG_6 monomer were evaluated by counting the number of diblock copolymers. The number of block copolymers increased with increasing monomer concentration, suggesting that both monomers were consumed at a comparable rate in the microflow (Figs. S21a and 21b).

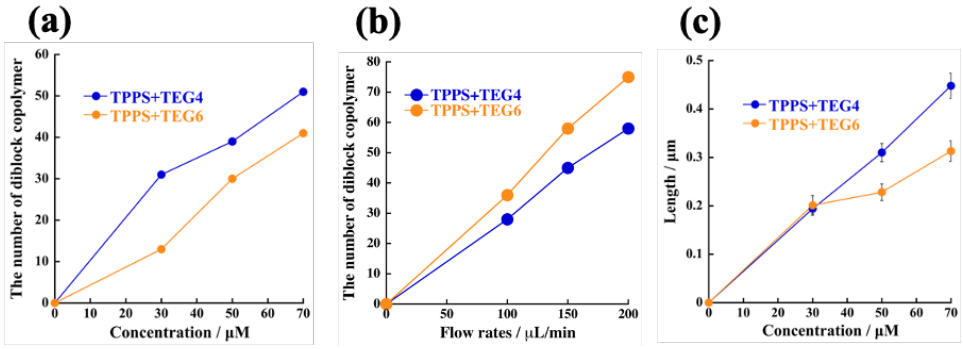

Fig. S21. Plots of the number of supramolecular diblock copolymers with respect to (a) monomer concentration and (b) flow rate, evaluated by counting 300 fibers in AFM images; (c) plot of the extended domain length in the diblock copolymer with respect to monomer concentration, measured from AFM images of 300 fibers; blue and orange lines correspond to supramolecular diblock copolymers obtained upon reaction with H_2TPPS_2-NHCO-EG_4 and -EG_6 monomer, respectively.

7. Effects of thermal diffusion of monomer on supramolecular copolymerization

To further confirm that the diffusion rates of monomers affect the efficiency of supramolecular copolymerization, the lateral layers including H_2TPPS_2-NHCO-EG_4 were selective heated by means of Peltier device as illustrated in Fig. S22 a. We confirmed that absorption at 490 nm increased with increasing the temperature of the Peltier device (Figs S22b and S22c). This result was evident that the diffused monomers from the lateral layer reacted at the end of H_4TPPS_4 supramolecular polymer in the central layer.

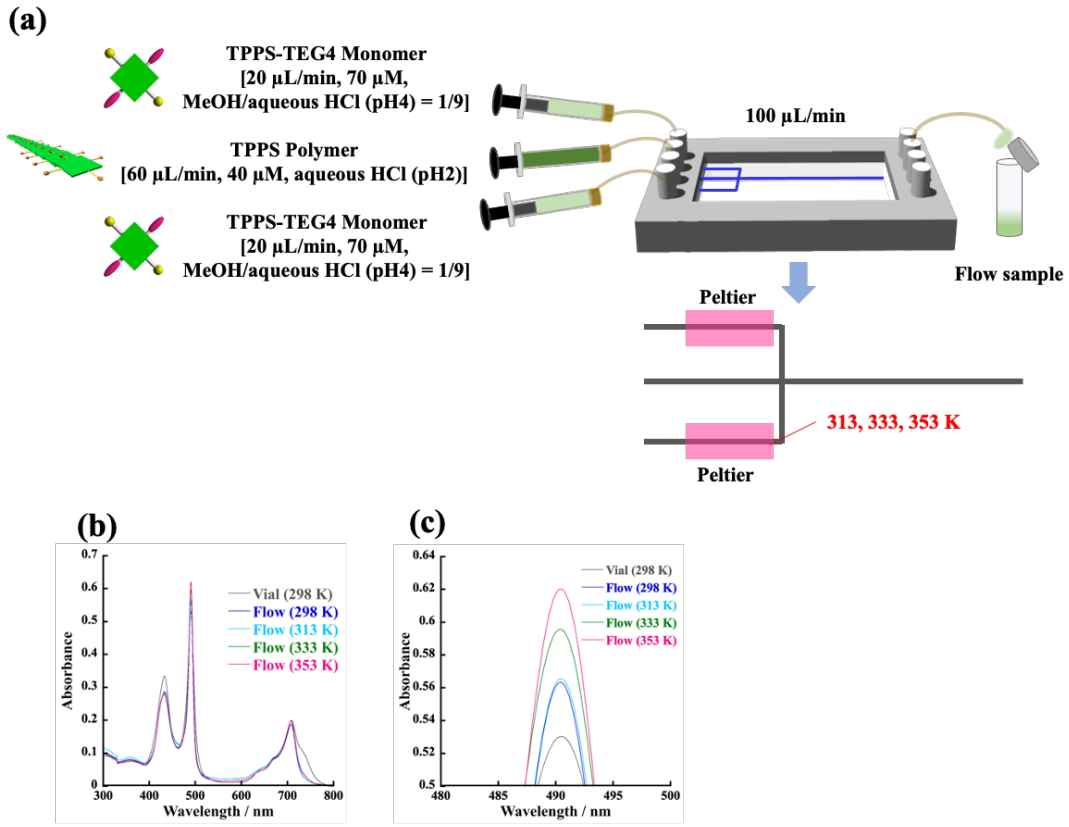

Fig. S22. (a) Schematic of microflow set-up for the present experiment using Peltier devices; heating effect of the lateral monomer (H_2TPPS_2-NHCO-EG_4) layers on the supramolecular copolymerization; (b) temperature-dependent UV–vis spectral changes of the eluted solution; (c) enlarged spectra of (b) [the inset values represent the temperature of the Peltier devices, 1.0 mm cell].

As a reference experiment, to investigate whether the heating treatment caused the decomposition of the parent H_4TPPS_4 supramolecular polymer in the central layer, we injected MeOH/water mixed solvent from the lateral inlets (without H_2TPPS_2-NHCO-EG_4 monomer), and heated the lateral channel by the Peltier device (Fig. S23 a). As a result, no significant effect of the heating on the stability of the supramolecular polymer (Fig. S23b).

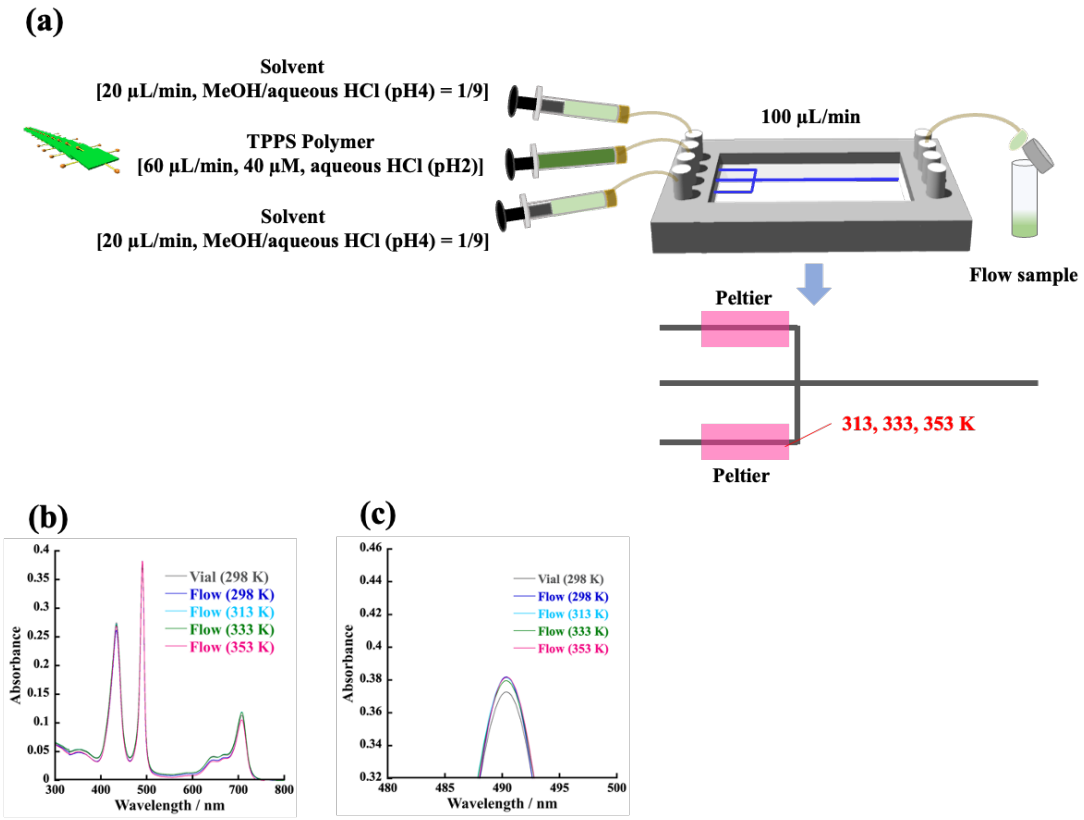

Fig. S23. (a) Schematic of microflow set-up for the reference experiment using Peltier devices; selective heating of the two lateral solvent layers; (b) temperature-dependent UV–vis spectral changes of the eluted solution; (c) enlarged spectra of (b) [the inset values represent the temperature of the Peltier devices, 1.0 mm cell].

No significant effect of the heating treatment on the homoaggregate of H_2TPPS_2-NHCO-EG_4 was also confirmed upon injection of solvent into the central channel (Fig. S24 a). Fig. S24 b was confirmed that no homoaggregate occurred in a microflow channel. The plots summarized in Fig. S24 c confirmed the clear correlation between the thermal diffusion of H_2TPPS_2-NHCO-EG_4 and the efficiency of the supramolecular copolymerization. From these experiments, it can be reasonably concluded that collision frequency plays an essential role for the present supramolecular copolymerization.

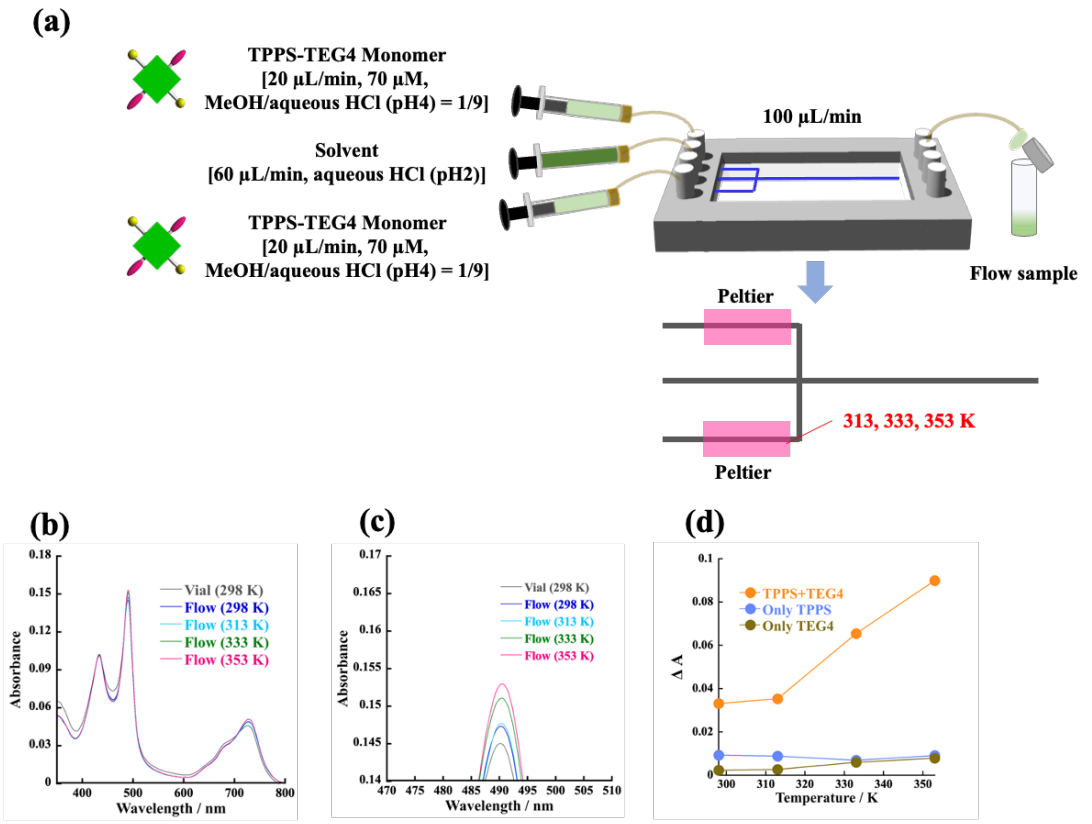

Fig. S24. (a) Schematic of microflow set-up for the reference experiment using Peltier devices; selective heating of the two lateral monomer layers; (b) temperature-dependent UV–vis spectral changes; (c) enlarged spectra of (b) [the inset values represent the temperature of the Peltier devices, 1.0 mm cell]; (d) ΔA at 490 nm versus temperature; orange line shows the effect of heating on the supramolecular copolymerization (data obtained from Fig. S22b); blue line represents data obtained from Fig. S23b: that is, upon sole injection of H_4TPPS_4 supramolecular polymer into the central inlets (without H_2TPPS_2-NHCO-EG_4 monomer); brown line represents data obtained from Fig. S24b; that is, upon sole injection of H_2TPPS_2-NHCO-EG_4 monomer into the side inlets (without H_4TPPS_4 supramolecular polymer).

8. References

1. C. Kanzaki, H. Yoneda, S. Nomura, T. Maeda and M. Numata, *RSC Adv*. **2022**, *12*, 30670.

2. C. Kanzaki and M. Numata, *Chem. Lett*. **2023**, *52*, 37.